Astron. Astrophys. 363, 1115–1122 (2000)

ASTRONOMY AND ASTROPHYSICS

Absorption spectra of Mg-rich Mg-Fe and Ca pyroxenes in the mid- and far-infrared regions

C. Koike[1], A. Tsuchiyama[2], H. Shibai[3], H. Suto[4], T. Tanabé[5], H. Chihara[2], H. Sogawa[1], H. Mouri[6], and K. Okada[6]

[1] Kyoto Pharmaceutical University, Yamashina, Kyoto 607-8412, Japan
[2] Osaka University, Department of Earth and Space Science, Toyonaka 560-0043, Japan
[3] Nagoya University, Department of Physics, Chikusa, Nagoya 464-01, Japan
[4] Subaru Telescope, National Astronomical Observatory of Japan, Hilo, Hawaii, USA
[5] The University of Tokyo, Institute of Astronomy, Mitaka, Tokyo 181-8588, Japan
[6] Meteorological Research Institute, Nagamine, Tshukuba 305-0052, Japan

Received 8 December 1997 / Accepted 6 October 2000

Abstract. Absorption spectra of the pyroxene group have been measured in mid and far infrared wavelengths. The samples are crystalline pyroxenes (enstatite, diopside, and natural pyroxene) and amorphous pyroxenes (enstatite and diopside glass). Especially, the synthetic pyroxenes such as orthoenstatite, clinoenstatite and diopside are pure and high-quality crystalline samples. For the first time we have detected very strong and sharp peaks at about 60–70 μm in the pyroxenes. The spectra of the pyroxenes are useful to identify the observed peaks, which have been detected by ISO on top of the broad amorphous silicates spectra of comets, circumstellar dust shells around both young stars and evolved stars. Compared to the broad features of amorphous pyroxenes, the crystalline pyroxenes show many sharp peaks in the mid and far infrared regions. Chemical composition, crystal structure, hydration, and temperature affect these spectra. The diopside may contribute to the emission feature of the planetary nebulae NGC 6302 in the far infrared region.

Key words: ISM: dust, extinction – infrared: ISM: lines and bands – stars: circumstellar matter – ISM: planetary nebulae: individual: NGC 6302

1. Introduction

The spectra of both evolved and pre-main-sequence stars, observed by ISO, revealed the presence of crystalline silicates such as olivines and pyroxenes in their circumstellar environments (Waters et al. 1996; Justtanont et al. 1996; Waters et al. 1998; Waelkens et al. 1996; Malfait et al. 1998; Molster et al. 1999a,b). The crystalline silicates were also found in many comets. The strong 11.25 μm emission peak, a characteristic feature of crystalline olivine, has been detected in comets, e.g. comet Halley (Bregman et al. 1987; Campins & Ryan 1989), Bradfield 1987S (Hanner et al. 1990), Levy 1990XX (Lynch et al. 1992), Mueller 1993a (Hanner et al. 1994b) and comet Hale Bopp (Crovisier et al. 1997; Wooden et al. 1999). In addition to the crystalline olivines, the presence of Mg-rich crystalline pyroxene has been confirmed by the detection of the 9.3 μm feature on top of the broad amorphous silicate spectrum in Comet Hale-Bopp (C/1995 01) (Wooden et al. 1999). In the far infrared region, the ISO spectrum also showed many crystalline silicate features (Crovisier et al. 1997) in comet Hale-Bopp. These spectra are very similar to those observed in the young star HD 100546 (Malfait et al. 1998), and in the evolved star AC Her (Molster et al. 1999b).

These detections provide important clues about the origin and evolution of crystalline dust in the circumstellar shells around young and evolved stars. This opens the possibility to detect various kinds of solid materials such as melilite, diopside and anorthite, which are expected from condensation theory (Grossman 1972; Tielens et al. 1998).

The observations of ISO show that amorphous silicates coexist with crystalline silicates in dust shells around young and evolved stars (Malfait et al. 1998; Molster et al. 1999a). Amorphous silicates are characterized by two broad bands at about 10 and 18 μm. Their shape and position is not constant. The silicate emission feature, which has been observed in the spectrum of the Taurus dark cloud source Elias 1 is broader, the FWHM is 4.3 μm, and peaks at a longer wavelength (10.6 μm) than the feature reproduced with the Trapezium emissivity (Hanner et al. 1994a).

In contrast to many observed spectra, laboratory data of crystalline silicates are rare in the literature (Steyer 1974; Koike et al. 1993; Koike & Shibai 1998; Jäger et al. 1998). In comparison with the measured spectra of olivine group with different Mg/Fe ratios, only two natural pyroxenes with complicated Ca-poor and Ca-rich compositions were measured (orthopyroxene and augite from Ichinome-gata; Koike et al. 1993). Interestingly, the spectra of the two natural pyroxenes show several sharp peaks around 9–11 μm and in the far-infrared region. Particularly in the far- infrared region the peak wavelengths are different from each other (Koike et al. 1993).

Send offprint requests to: C. Koike
Correspondence to: koike@cr.scphys.kyoto-u.ac.jp

In this paper we present the absorption spectra of various pyroxenes with Ca-poor and Ca-rich compositions including synthetic and natural pyroxenes to study whether the 9.3 μm peak is generally common or not in pyroxenes. We also investigated systematic changes in the peak wavelengths according to the crystalline state and/or chemical composition.

With regard to synthetic pyroxenes, three kinds of pyroxenes, i.e. orthoenstatite $MgSiO_3$, clinoenstatite $MgSiO_3$, and diopside $CaMgSi_2O_6$, were synthesized. These pure and high-quality crystalline samples are very important to study the correlation between the band shifts and chemical composition.

As for amorphous silicates, the measured spectra of the amorphous pyroxenes show different features; amorphous enstatite (Stephens & Russell 1979), amorphous bronzite (Dorschner et al. 1988), pyroxene glass (Jäger et al. 1994), and amorphous enstatite (Brucato et al. 1999) have broad bands at respectively 9.1 μm, 9.5 μm, 9.5 μm, and 9.89 μm. An amorphous pyroxene measured by us also shows a broad band at 9.5–9.7 μm (Koike & Tsuchiyama 1992). The feature in the spectrum of the pyroxene glass satisfactorily matches those observed in the spectra of the Orion Trapezium and massive young stellar objects (YSOs) in molecular clouds (Jäger et al. 1994). These amorphous pyroxene samples, except ours, show a broad band at about 17–19 μm. Our amorphous pyroxenes show a broad band at bout 22–23 μm.

In this work, we obtained new amorphous pyroxenes, synthesized by the quenching method. We also investigated the shift of the peak position of the 18 μm band after hydration of the amorphous pyroxenes. This study is important if we consider the history of cometary dust or interstellar/circumstellar dust especially based on the fact that mixture of amorphous silicates, crystalline silicates and water ice exist around young (Malfait et al. 1998) and evolved stars (Molster et al. 1999a; Lim et al. 2000).

2. Measurements

2.1. Sample preparation

Pyroxenes have the general formula, $M_2T_2O_6$. In the Ca-Mg-Fe pyroxenes, the M site is occupied mainly by Mg, Fe, and Ca, and T by Si (Al can also be incorporated into M and T sites as a minor element). These pyroxenes are divided into sub divisions (Morimoto et al. 1988); the Mg-Fe pyroxenes (or Ca-poor pyroxenes) with the end members of enstatite $MgSiO_3$ (En) and ferrosilite $FeSiO_3$ (Fs), and the Ca pyroxenes (Ca-rich pyroxenes) with the end members of diopside $CaMgSi_2O_6$ (Di) and hedenburgite $CaFeSi_2O_6$ (Hd). Their chemical composition are expressed by using the end components of En, Fs and Wo (wollastonite $CaSiO_3$).

The crystalline and amorphous pyroxenes used in the present measurements are listed in Table 1. The crystalline samples are one Ca-rich (diopside) and three Ca-poor pyroxenes (orthoenstatite, clinoenstatite, and orthopyroxene). The orthoenstatite ($MgSiO_3$) crystals were synthesized by the flux method, i.e. single crystals of orthoenstatite were grown from a melt in the system $MgO-SiO_2-Li_2O-MoO_3-V_2O_5$ (Ozima 1982). The contamination of the flux components LiO_2, MoO_3 and V_2O_5 is negligible (< 0.5 wt.%) and does not affect the infrared spectrum as we compared the spectra of the flux with those of the samples. The clinoenstatite crystal ($MgSiO_3$) was converted from the orthoenstatite crystal; the orthoenstatite crystal was heated to 1100-1200 °C, above the protoenstatite-orthoenstatite transition point of 985 °C, for a few hours in air and afterward quenched into water. The product became clinoenstatite crystals with polysynthetic twinning, which showed a typical texture formed by rapid transformation from protoenstatite. Another Ca-poor pyroxene used is natural orthopyroxene from Bambel, Norway. The composition has been determined by an EPMA (electron probe microanalyzer) (JEOL733) at Osaka University and is $(Mg_{1.721}Fe_{0.170}Mn_{0.004}Ni_{0.002}Ca_{0.022}Na_{0.001}Al_{0.060}Ti_{0.004})(Si_{1.918}Al_{0.082})O_4$, or $(En_{89.9}Fs_{8.9}Wo_{1.2})$.

Table 1. Crystalline and amorphous pyroxene samples used in the present study.

Sample	Chemical composition	Crystal system	Natural/Synthetic
Clinoenstatite	$MgSiO_3$	monoclinic	Flux-grown/reheated
Orthoenstatite	$MgSiO_3$	orthorhombic	Flux-grown
Orthopyroxene	$En_{89.9}Fs_{8.9}Wo_{1.2}$ *	orthorhombic	Bambel, Norway
Diopside	$Wo_{46}En_{54}$ *	monoclinic	CZ-grown
Enstatite glass	$MgSiO_3$	amorphous	Quenched melt
Enstatite gel	$MgSiO_3$	amorphous	Sol-gel method
Diopside glass	$CaMgSi_2O_6$	amorphous	Quenched melt

* En : $MgSiO_3$, Fs : $FeSiO_3$, Wo: $CaSiO_3$

The diopside crystal was synthesized by the CZ (Czochralski) method, i.e. a single crystal of diopside grown from its melt by pulling a seed crystal (Takei et al. 1982). The crystal is slightly nonstoichiometric, and has the chemical formula $Ca_{0.92}Mg_{1.08}Si_2O_6$, that is, $(Wo_{46}En_{54})$.

Two of the amorphous samples have an enstatite and one has a diopside composition. The enstatite glass ($MgSiO_3$) and the diopside glass ($CaMgSi_2O_6$) were synthesized by melting mixtures of reagent-grade MgO, SiO_2 and $CaCO_3$ (the carbonate was decarbonated during heating) in air and quenched into water. The samples are almost stoichiometric in composition. Another amorphous enstatite (enstatite gel) was formed by a gelling method (Hamilton & Henderson 1968). No crystalline feature was detected in X-ray diffraction patterns.

2.2. The procedure of measurements

The bulk samples were crushed and ground in an agate mortar. Large size particles were removed by sedimentation in alcohol. The size of the particles, measured with the SEM (scanning electron microscope) is smaller than 0.5 μm and 1 μm in the mid-infrared region and far-infrared region respectively. These fine particles were dispersed in KBr pellets and polyethylene (PE) sheets. The transmission of the pellets and sheets were measured with the Fourier transform infrared spectrometer JASCO FT/IR-350 (resolution; 0.5 cm^{-1}) in the mid- and far-infrared

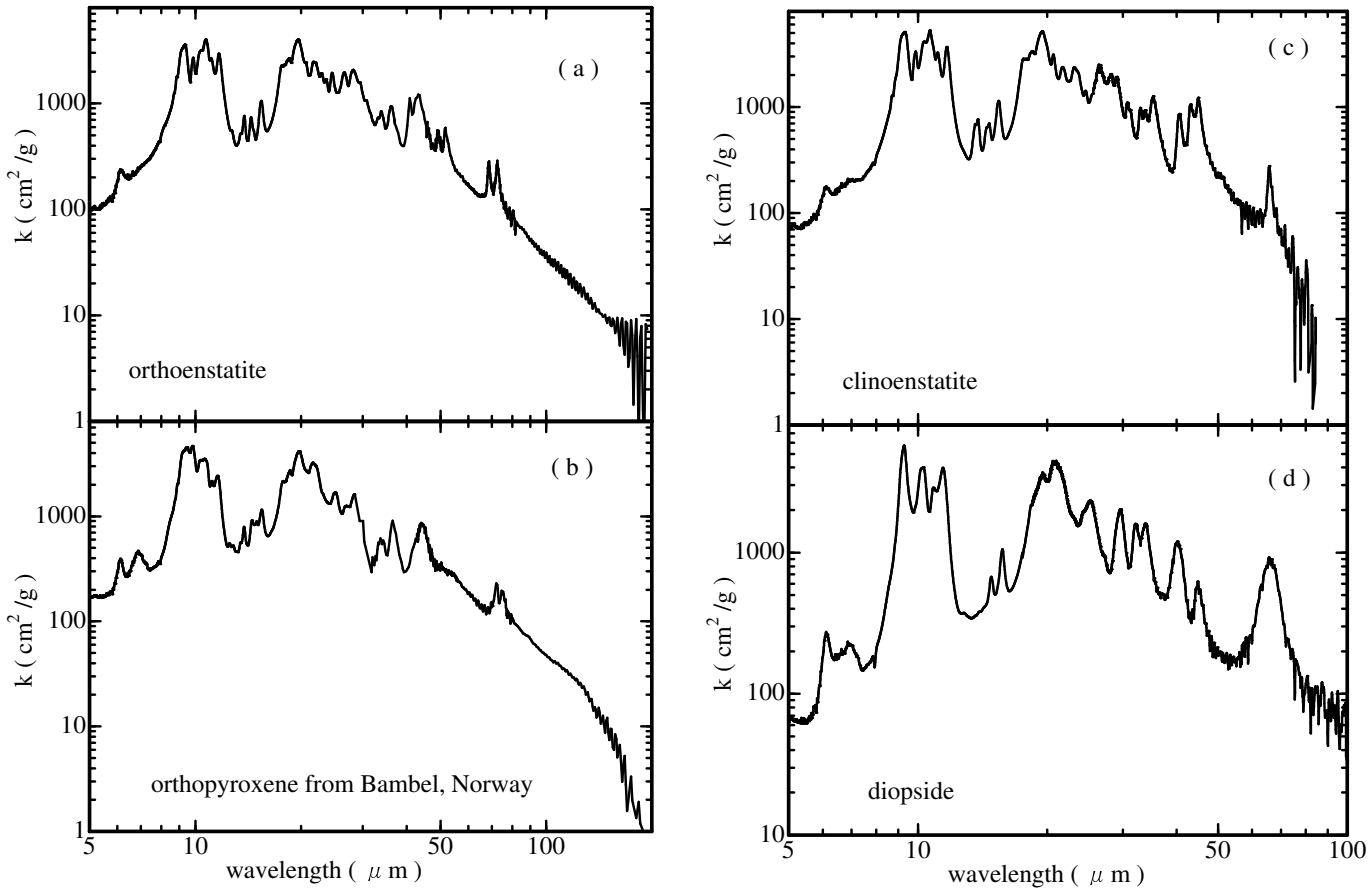

Fig. 1a–d. The mass extinction coefficients of present crystalline pyroxenes; **a** orthoenstatite, **b** orthopyroxene from Bambel, Norway, **c** clinoenstatite, and **d** diopside.

regions, and with the BOMEM DA3 (resolution; 1.0 cm^{-1}) at the Institute of Space and Astronautical Science (ISAS) (at Sagamihara, Kanagawa, Japan) in the far infrared region.

The mass extinction coefficient, κ, was derived from the transmittance, T, of pellets and sheets as follows (Koike et al. 1989):

$$\kappa = \left(\frac{S}{M}\right) \ln\left(\frac{1}{T}\right),$$

where S is the surface area of a KBr pellet or polyethylene sheet, and M is the mass of the sample embedded in the sample pellet or sheet.

The alteration of the amorphous samples (enstatite glass, enstatite gel and diopside glass) due to hydration was examined by infrared spectroscopy up to 40 μm. The hydration proceeded through the following steps. The KBr pellet containing sample particles was dissolved into water and kept at room temperature for 48 hr. After that, the solution containing sample particles was heated at 90 °C for 7 hr in order to evaporate water. The residue (KBr and sample particles) was reheated at 120 °C for 19 hr in order to dry up thoroughly. The recovered mixture of KBr and sample particles was ground down and re-pressed into a pellet.

3. Results

3.1. Crystalline pyroxenes

The spectra of the pyroxenes are shown in Fig. 1. The absorption spectra of the present samples vary considerable and differ from those of the two natural pyroxenes from Ichinome-gata previously measured (Koike et al. 1993). Based on the chemical compositions of pyroxenes, we divided these spectra into three groups, namely pure enstatite (synthetic orthoenstatite and synthetic clinoenstatite; the Mg end member of pyroxene), orthopyroxene (orthopyroxene from Bambel and from Ichinome-gata; Mg-rich but contains small amounts of Fe, Al and Ca) and Ca-rich pyroxene (synthetic-diopside and natural-augite from Ichinome-gata; Ca $\approx$ 0.9–1.0 and Mg $\approx$ 0.9–1.0 with O = 6). In the mid infrared region, the peak positions are blue shifted for about 0.1 μm compared to the data measured by the previous low resolution spectrometer Shimadzu IR-27G (Koike & Shibai 1998). Although the peak wavelengths of the corresponding features are different, the spectrum of each group has similar features. In the pure enstatite group, the spectra are not so much dependent on the type of crystal structures (ortho or clino) in the mid infrared region, but the peaks of the clinoenstatite in the mid infrared region become about 30% stronger than those of the orthoenstatite. In the far infrared region the

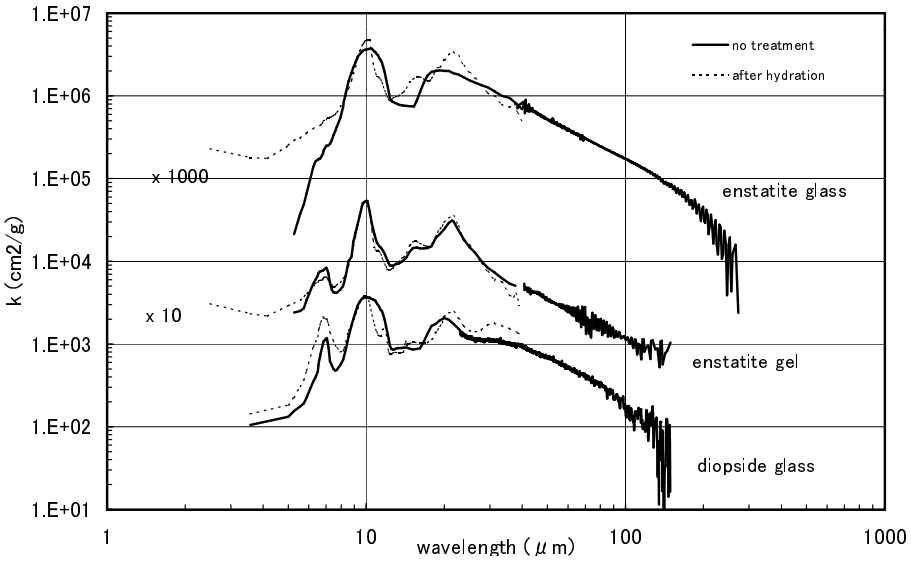

Fig. 2. The mass extinction coefficients of the amorphous pyroxenes; diopside glass, enstatite gel, and enstatite glass, which are multiplied by 1, 10, and 10^3 respectively. The dotted lines represent the spectra after hydration.

peaks become different. In the case of Ca-rich pyroxenes, the three strong peaks in the 10 μm region are very similar for the synthetic and the natural samples. Diopside has a strong and broad peak at about 66 μm. This peak is about 50% stronger than the peak of natural augite. Natural augite has a degenerate band at 33 μm and only a very weak peak at 45 μm compared to diopside. As for the case of the natural orthopyroxenes, the two spectra are similar. However, the two peaks at 70 μm are very strong in the Norway sample compared to the very weak band for the Ichinome-gata sample.

Many sharp peaks appear not only in the mid-infrared region, but also in the far-infrared region. The peak wavelengths of the present samples are listed in Table 2, together with those of the two previous samples (Koike et al. 1993). The enstatite group shows sharp peaks compared with the orthopyroxenes, which has slightly broader or degenerate bands.

Three strong absorption peaks appear in the 9–12 μm region for each sample, although the strength of the peaks depends on the sample as is shown in Fig. 1. The 9.3 μm feature is detected in all pyroxenes. The 20 μm feature also varies in the shape, width and peak position. The peak positions of the clino- and ortho-enstatite samples are about 19.7–20 μm. The synthetic diopside and natural orthopyroxene show double peaks at 20 and 21 μm.

The synthetic orthoenstatite and natural orthopyroxene from Bambel show many strong peaks in the far-infrared region compared with the two natural pyroxenes from Ichinoeme-gata, and interestingly the bands of the orthoenstatite at 42, 50 and 70 μm clearly appear as double bands.

As for the 32.8 μm peak of the orthoenstatite, the present data shows a weaker peak, about 2.5 times, than the data of the orthoenstatite (Koike & Shibai 1998) in spite of the fact that it is the same material. This might be due to differences in the shape distribution for each sample, although the exact reason is not clear.

In summary, the sharp peaks of pyroxene appear very distinctly at 25, 28–29, 33–36, 40–45, 50, and 66–75 μm.

3.2. Amorphous pyroxenes

The three samples show two broad bands near 10 and 20 μm as is shown in Fig. 2.

The 20 μm band of the present samples is changed due to hydration and shifts to 21.7 μm (thin dotted lines in Fig. 2); the 20 μm band of amorphous olivine was also changed by hydration and annealing (Koike et al. 1992). The peak positions of the present samples before and after hydration are listed in Table 3. The extinction coefficients of the enstatite glass and enstatite gel follow a power law with $\lambda^{-1.6}$ and $\lambda^{-1.5}$, respectively, in the wavelength range of 30–100 μm, and those of the diopside glass have a power law with $\lambda^{-1.8}$ in the wavelength range of 45–100 μm. The enstatite glass shows a sharp decrease, which is proportional to $\lambda^{-(3-4)}$, in the far-infrared wavelength region above 140 μm.

4. Discussion

4.1. Synthesized samples

Our synthesized samples are pure and large high-quality single crystals. Compared to our samples, the synthesized enstatite sample by Jäger et al. (1998) is micro crystalline; they formed $MgSiO_3$ melt at 1700 °C, and cooled it to room temperature at 10^3 K/hr. At such high cooling rate, small and highly imperfect crystals of clinoenstatite, which were transformed from the high-temperature phase (protoenstatite), should be formed. Moreover, also forsterite (Mg_2SiO_4) and silica (SiO_2) were formed as a result of incomplete peripheral reaction between forsterite and melt. In contrast, we synthesized single crystals of orthoenstatite, which is the stable phase of $MgSiO_3$ at room temperature and 1 atm., with the flux method (Ozima 1982). If enstatite is synthesized at temperature higher than 985 °C, protoenstatite is formed, and this transforms to clinoenstatite having polysynthetic twinning as a metastable phase by rapid cooling (e.g., Heubner 1980), and orthoenstatite cannot be obtained. This is the reason why we used the flux method at low tempera-

Table 2. The peak wavelengths of the present crystalline samples (μ m).

Pure enstatite (synthetic)		Orthopyroxene (natural)		Ca-rich pyroxene	
Clino-enstatite	Ortho-enstatite	Bambel, Norway	Ichinome-gata, ‡‡	Diopside, synthetic	Augite, natural, Ichinome-gata ‡‡
7.1		6.9			6.9
7.3		7.2	7.2	7.2	7.2
8.7	8.9			7.9	7.8
9.34	**9.34**		**9.24**	**9.28**	**9.29**
		9.47			
9.88	9.87	**9.82**			
			9.78		
10.34*		10.34	**10.53**	**10.29**	**10.25**
10.66	**10.70**	**10.62**			
			11.12	10.86*	
11.12*	11.09*	11.14*			**11.35**
			11.58	**11.43**	
11.68	**11.68**	**11.57**			
	12.69	12.53*		12.80	
13.61	13.45	12.82	13.81		
		13.47			
13.81	13.79	13.77			
	14.42		14.49		
		14.50		14.82	
14.648		14.94			14.82
15.41	15.41		15.46	15.76	15.69
		15.74			
	17.63*	17.73			
17.61*	17.9*	18.62*			
18.44*	18.54		18.44		
19.48			**19.48**	**19.49**	**19.29**
	19.60	**19.74**			
20.64	20.62			**20.60**	**20.64**
21.70	21.70	**21.63**	21.58		
	22.87				
23.12	23.60			24.3	
24.61	24.5	25.02		**25.1**	**24.26**
26.56	26.58	26.97			
				27.04	
28.1	**28.2**	**28.45**	**28.5**		
28.9					
	29.4	30		**29.6**	**29.5**
30.8	30.6			32.1	**32.3**
33.03	**33.2**	33.7		**33.9**	**33.7**
33.84	**33.9**				
35.3					
	36.1	**36.5**	**36.2**		
40.7	**40.8**			40.1	**39.9**
43.12	**43.20**				
44.9		**43.9**	**44**	44.8	44.2*
	49.02		49*		
50	**51.6**	50	53*		
65.7	**68.7**			**65.7**	**66.5**
	72.5	**72.0**			
		74.6			

bold numbers: strong peaks

*: very weak peaks

‡‡: the previous data in far infrared region (Koike et al. 1993)

Table 3. The peak positions of the amorphous pyroxenes (μ m).

Diopside-glass		Enstatite-glass		Enstatite-gel	
Starting	Hydration ‡	Starting	Hydration ‡	Starting	Hydration ‡
7.04	6.80			7.02	6.94
10.21	9.90	10.42	10.21	10.05	10.0
	11.8*				
	12.2*				
14.29	14.20*				
	15.27*		16.0*	15.63*	15.39
20		19.23			
	21.74		21.74	21.41	21.74
30.86	31.25				32*
				45*	

‡ : spectra longer than 40 μ m are not measured.

ture below 985 °C in stead of using the CZ or FZ (floating-zone) method, which can grow larger and more perfect single crystals from their own melts without incorporating impurities (of flux). We applied very slow cooling rates (as slow as 0.2 K/hr) to obtain large and clear single crystals (up to 2 cm in length).

4.2. Spectra of samples

In general, there is a shift of the peak wavelengths of about 0.2–0.3 μm, when spherical particles are in a medium instead of vacuum (Schmidt 1981). The shape of the crystalline silicates such as pyroxenes and olivines were observed under an SEM. They all show irregularities and clearly differ from spheres. The particles of our pyroxenes and forsterites are dispersed on bulk materials (KBr, PE, NaCl, Ge, Si, etc) after which the spectra are measured in mid and far infrared region. The peak positions are nearly the same in a medium as in the air although the peak strengths are a little changed due to irregularity in shapes. In the case of an irregular shape, the medium effects on the peak positions are minor. The same result was found by Colangeli et al. (1995).

As a next step, calculated spectra of spherical particles are compared to the calculated spectra of particles with a continuous distribution of ellipsoids (CDE; Bohren & Huffman 1983) using our derived optical constants of bulk samples (En, Fo100, Fo90, and Fa) (Sogawa & Suto et al. in preparation). Clearly these spectra are different. The calculated spectra of CDE in a medium are very similar to those in vacuum, but the strength of the peaks are higher by n (medium index) times the vacuum values. The calculated spectra of CDE in medium are similar to the measured spectra of fine particles of En, Fo100 and Fo90 (Sogawa et al. 1999; Jäger et al. 1998). Therefore, it is unnecessary to consider the shift of the peak positions measured in medium and in vacuum.

The results of the enstatite samples are similar to those of Jäger et al. (1998) except for some peaks in the far-infrared region. In spite of the low resolution, our measured spectra of the orthoenstatite clearly show the two strong peaks at about 70 μm. The existence of these sharp and clear features are confirmed for the first time in the far infrared region. The two peaks also clearly appear in the calculated CDE spectrum of natural enstatite reported by Jäger et al. (1998). The discrepancy may be due to the difference in the dispersion of the particles in PE sheets and the difference in quality of crystals.

In contrast to the spectra of the amorphous pyroxenes in this paper with two broad bands at about 10–10.4 μm and 19.2–21.4 μm, the spectra of the glassy bronzite, pyroxene glass, and amorphous enstatite showed two broad bands at 9.5 and 18.5 μm (Dorschner et al. 1988), 9.5 and 18.8 μm (Jäger et al. 1994), and 9.89 and 19.21 μm (Brucato et al. 1999), respectively. The difference in the spectra between our amorphous pyroxenes and their glass might be due to the procedure for preparation, that is, the peak positions are strongly influenced by the quenching method (Jäger et al. 1994), or difference of the chemical compositions (the glasses contain Fe elements in the previous study, but not in this study).

4.3. Comparion with observed spectra of the 7 μm band

In oxygen-rich circumstellar shells, the 7 μm band was observed to be correlated with dust, and this carrier remains to be identified (Goebel et al. 1994). In this work, the 7 μm band is detected in the spectra of the crystalline pyroxenes (the clinoenstatite, diopside, natural orthopyroxene from Bambel and Ichinome-gata, and augite), the diopside glass and the enstatite gel, but only marginally in the enstatite glass. It is not clear if this band is due to some impurity (possible contamination during preparation for the measurements of spectra). The 7 μm band appears only as a hump in the clinoenstatite (crystalline silicates) which does not contain Ca. On the other hand, as for the diopside glass, the 7 μm band becomes stronger after hydration. In this case, this 7 μm band may be due to Ca contained materials, such as carbonates glass in the diopside glass (Knacke & Krätschmer 1980).

4.4. Comparion with observed spectra NGC 6302

In connection with Ca-containing mineral, the spectra of diopside are compared with the ISO observation of the planetary nebula NGC 6302 (Lim et al. 2000). The spectrum of NGC 6302 is characterized by very strong and narrow forbidden emission lines and many relatively sharp features due to crystalline silicates (see Fig. 3). The 43 μm feature and the strong and very broad emission feature peaking at about 65 μm are proposed to be identified with crystalline ice of 45 K (Barlow 1998; Lim et al. 2000). The observed peak position of 65 μm is however at a little longer wavelength than those of laboratory measurements of ice (Smith et al. 1994).

The strong and broad peak of 65 μm of NGC 6302, is similar to the spectrum of crystalline diopside multiplied by a 50 K Planck function. However, the peak position is not exactly the same and has a difference of about 1 μm from the laboratory spectrum of diopside. Our recent measurements of spectra at liquid He temperature show that the peak position shifts about 1 μm to the shorter wavelengths compared to the peak position of 65.7 μm, measured at room temperature (Chihara et al. 2000). Further, the spike at about 68.93 μm of NGC 6302 might be due to forsterite (Barlow 1998; Lim et al. 2000). This

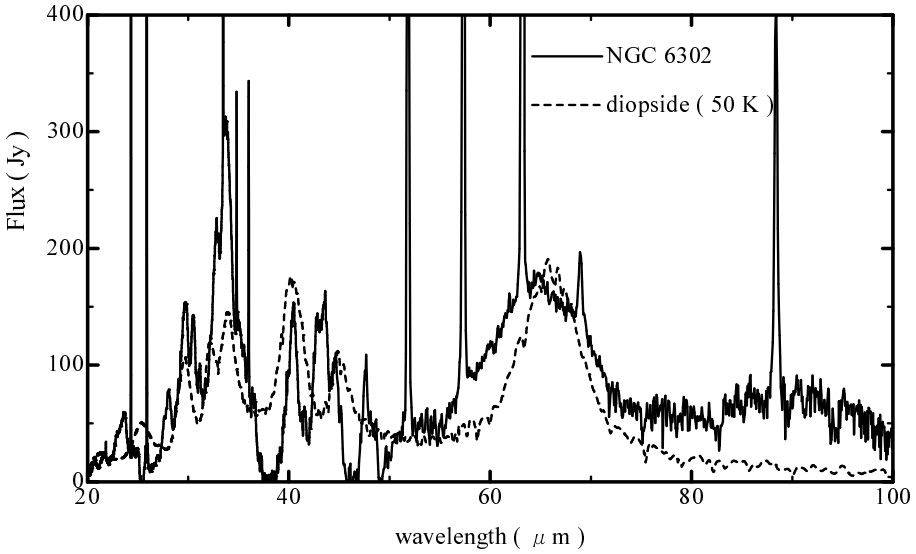

Fig. 3. Comparison of the continuum subtracted spectrum of NGC 6302 with the spectrum of diopside multiplied by a Planck curve of 50 K (arbitrary scale). The very narrow and strong features are forbidden emission lines.

is strongly supported by our recent measurements that forsterite has a sharper and stronger peak at liquid He temperature and that the peak positions in far infrared region shift to shorter wavelengths by about 1–0.3 μm compared the spectra at room temperature, i.e. the feature at 69.6 μm shifts to 68.8 μm. When crystalline pyroxenes and forsterite are cooled down to liquid He temperature, the spectra show sharper and stronger peaks, which also shift to shorter wavelengths compared to those at room temperature (Chihara et al. 2000). This is similar to the result of Mennella et al. (1998). Looking into the another peaks in Fig. 3, the observed peaks at 30, 34, 40, and 45 μm are also very similar to the peaks of the diopside at room temperature.

The chemical abundances of NGC 6302 show that Mg, Al, Ca, and Fe are depleted in gas. In particularly, Ca is a factor of 100 less abundant with respect to the Sun and B stars. These elements may be in the form of dust (Pottasch & Beintema 1999). Considering the depletion of the elements in the gas, the presence of Ca-rich pyroxene $(\mathrm{Ca,Mg})\mathrm{SiO_3}$ might be possible. Most peaks of NGC 6302, can be identified with diopside, crystalline water ice and forsterite. The broadness of the observed band at 65 μm indicates a blend of diopside and crystalline water ice.

Many new emission peaks at wavelengths between 20 and 45 μm have been detected in dust shells around evolved oxygen-rich stars and young stars (ISO results) (Molster 2000). Crystalline silicates such as olivines and pyroxenes are attributed to most of these emission peaks. These identifications are reasonable based on the present measurements. For example, the detected peak at 40.5 μm in HD 100546 (Malfait et al. 1998), He 2-113 and BD+30 3639 (Waters et al. 1998) is due to crystalline pyroxene, and this band commonly appears in the spectra of synthetic enstatite and Ca-rich pyroxene (diopside and augite). Crystalline water ice is tentatively identified with the 43 μm hump (Waters et al. 1996; Molster et al. 1999a). Furthermore, by adding these identifications, we indicate pyroxenes as another promising candidate for the carriers of humps at about 43–44 μm. Pyroxenes (ortho-enstatite, orthopyroxene from Bambel, and orthopyroxene from Ichinome-gata) have a strong band at 43–44 μm. Still more, the detection of the double peaks at about 50 and about 70 μm may confirm the identification of pyroxene group same as forsterite detected at about 69 μm in the young star HD 100546 (Malfait et al. 1998) and NGC6302 (Lim et al. 2000).

The spectra of diopside and enstatite glasses have a very broad band at around 10.0–10.3 μm with a half-width of about 3 μm. These spectra are similar to the spectrum of Elias 1, but show a peak at slightly shorter wavelength than the spectrum of Elias 1; the spectrum shows peak at about 10.6 μm with half-width of about 4.6 μm, which might be due to large particles (Hanner et al. 1994a).

In this paper, we investigate the spectra of only Fe-poor Mg-Fe-Ca pyroxenes. We will further investigate the spectra of Fe-rich pyroxene, and make clear the correlation between the band and chemical composition in the near future.

Acknowledgements. We thank Prof. H. Takei of Osaka University, Prof. M. Ozima of University of Tokyo, Dr. S. Tachibana of Osaka University, Dr. M. Shimobayashi of Kyoto University for preparing diopside crystal, orthoenstatite crystals and enstatite gel used in the present study. We also warmly thank Prof. L.B.F.M. Waters and Dr. F.J. Molster of University of Amsterdam for kindly providing us with their ISO data of NGC 6302, AFGL 4106, HD 100546, and BD + 30369. We are grateful to Dr. F.J. Molster for critical reading of the manuscript and many helpful suggestions. We thank Prof. H. Okuda of ISAS for his continuous encouraging to us in this work and for his careful reading of this paper. This work was supported by the Grant-in-Aid of Japanese Ministry of Education, Science, and Culture (11134210), and ISAS.

References

Barlow M.J., 1998, Ap&SS 255, 315
Bohren C.F., Huffman D.R., 1983, Absorption and scattering of light by small particles. John Wiley and Sons Inc., New York
Bregman J.D., Witteborn F.C., Wooden, et al., 1987, A&A 187, 616
Brucato J.R., Colangeli L., Mennella V., et al., 1999, A&A 348, 1012

Campins H., Ryan E.V., 1989, ApJ 341, 1059
Chihara H., Koike C., Tsuchiyama A., 2000, PASJ submitted
Colangeli L., Mennela V., Di Marino C., et al. 1995, A&A 293, 927
Crovisier J., Leech K., Bockelee-Morvan Brook T.Y., et al., 1997, Sci 275, 1904
Dorschner J., Friedemann C., Gürtler J., Henning T., 1988, A&A 198, 223
Goebel J.H., Bregman J.D., Witteborn F.C., 1994, ApJ 430, 317
Grossman L., 1972, Geochimica et Cosmochimica Acta 36, 597
Hanner M.S., Brooke T.Y., Tokunaga A.T., 1994a, ApJ 433, L97
Hanner M.S., Hackwell J.A., Russell R.W., Lynch D.K., 1994b, Icarus 112, 490
Hanner M.S., Newburn R.L., Gehrz R.D., et al., 1990, ApJ 348, 312
Hamilton D.L., Henderson C.M.B., 1968, Mineral. Mag. 36, 832
Heubner J.S., 1980, In: Prewitt C.T. (ed.) Review in Mineralogy vol.7, Pyroxenes. Mineralogical Society of America, p. 213
Jäger C., Mutschke M.H., Begemann B., et al., 1994, A&A 292, 641
Jäger C., Molster F.J., Dorschner J., et al., 1998, A&A 339, 904
Justannont K., de Jong T., Helmich F.P., et al., 1996, A&A 315, L217
Knacke R.F., Krätschmer W., 1980, A&A 92, 281
Koike C., Shibai H., 1998, ISAS report no. 671
Koike C., Tsuchiyama A., 1992, MNRAS 255, 248
Koike C., Hasegawa H., Asada N., Komatuzaki T., 1989, MNRAS 239, 127
Koike C., Shibai H., Tsuchiyama A., 1993, MNRAS 264, 654
Lim T., Molster F.J., Sylvester R.J., et al., 2000, A&A in press
Lynch D.K., Russell R.W., Hackwell J.A., et al., 1992, Icarus 100, 197
Malfait K., Waelkens C., Waters L.B.F.M., et al., 1998, A&A 332, L25
Mennella V., Brucato J.R., Colangeli L., et al., 1998, ApJ 496, 1058
Molster F.J., Waters L.B.F.M., Trams N., et al., 1999a, A&A 350, 163
Molster F.J., Yamamura I., Waters L.B.F.M., et al., 1999b, Nat 401, 563
Molster F.J., 2000, Ph.D. Thesis, University of Amsterdam
Morimoto N., et al., 1988, Amer. Mineral. 73, 1123
Ozima M., 1982, J. Jpn. Assoc. Mineral. Petrol. Economic Geology, Spec. Issue No. 3, 97 (in Japanese)
Pottasch S.R., Beintema D.A., 1999, A&A 347, 975
Schmidt R., 1981, Astron. Nachr. 302, 235
Smith R.G., Robinson G., Hyland A.R., Carpenter G.L., 1994, MNRAS 271, 481
Sogawa H., Kozasa T., Koike C., Suto H., 1999, Proceedings of the 32nd ISAS Lunar and Planetary Symposium 32, 179
Stephens J.R., Russell R.W., 1979, ApJ 228,780
Steyer T.R., 1974, Ph.D. Thesis, University of Arizona
Takei H., Miura T., Morioka M., 1982, J. Crystal Growth 60, 453
Tielens A.G.G.M., Waters L.B.F.M., Molster F.J., Justtanont K., 1998, Ap&SS 255, 415
Waelkens C., Waters L.B.F.M., de Graauw M,S., et al., 1996, A&A 315, L245
Waters L.B.F.M., Molster F.J., de Jong T., et al., 1996, A&A 315, L361
Waters L.B.F.M., Beintema D.A., Zijlstra A.A., et al., 1998, A&A 331, L61
Wooden D.H., Harker D.E., Woodward C.E., et al., 1999, ApJ 517, 1034